ORIGINAL PAPER

Characterizing Anisotropic Rocks Using a Modified St. Venant Method and High-Resolution Core Measurements with Extension to Field Logs

D. Sassen[1] · B. Abell[1]

Abstract

Hydraulic fracture modeling has progressed into a high impact decision-making tool for the unconventional petroleum industry. However, the main influence on the model results are the rock mechanical inputs, typically derived from field logs and supplemented by core measurements, and the uncertainty associated to these. The strongly layered nature of unconventional mudstones, however, requires representation of the high contrast in properties between layers, and their anisotropic elastic behavior. This investigation provides an integrated method for experimentally measuring elastic mechanical properties from new anisotropic ultrasonic measurements at sufficiently high resolution (cm scale) to honor the rock fabric along with triaxial compressional data on sample plugs. These results are analyzed, compared, and integrated using a newly developed methodology, based on St. Venant's reduced symmetry approximation, to develop a continuous representation of the elastic properties and their associated uncertainties. For cases where core is not available, we provide a method to reconstruct anisotropic properties at cm resolution using standard resolution field logs and a borehole image log. A case study on a core from the Permian basin is presented and verified against a standard workflow. Additionally, the methodology to propagate from the cored well to nearby regions (e.g., formations above the cored interval) is demonstrated for cases where logs are available, but core data are not.

List of Symbols

Indices (i, j) can be either 1 or 3 (horizontal of vertical)

C_{ij} — Stiffness tensor terms (Voigt notation)
S_{ij} — Compliance tensor terms (Voigt notation)
E_i — Young's modulus
v_{ij} — Poisson's ratio
v — Poisson's ratio—Saint Venant 3-term
v_i — Poisson's ratio—Saint Venant 4-term
G_{ij} — Shear modulus
ρ — Density
σ_i — Stress
K_0 — Horizontal to vertical stress ratio

Index i can be V, H, or 45 for vertical, horizontal and 45° propagation, respectively

$V_{\mathrm{P}i}$ — P-wave velocity
$V_{\mathrm{s}i}$ — S-wave velocity

✉ D. Sassen
doug.sassen@wdvglab.com

1 W.D. Von Gonten Laboratories, Houston, TX, USA

x_i — Model parameters ($i = 1…N$)
$m(x_i)$ — Model results as function of x
d — Observed data ($i = 1…N$)
Σ — Data covariance matrix
$L(x_i)$ — Unnormalized log-likelihood
$|\psi|$ — Structural constraint
H — Point spread function
z — Latent model parameters
$^{-1}$ — Matrix inverse
$^{\mathrm{T}}$ — Transpose
$*$ — Convolution
U — Left singular matrix
V — Right singular matrix

1 Introduction

The petroleum industry has progressed to making high impact decisions on fracture placement, fluid pumping schedules, and fracture sequencing based on hydraulic fracture modeling, especially in unconventional reservoirs. The main influence on these hydraulic fracturing models is the

rock mechanical inputs (e.g., elastic moduli), their effect on stress, and the uncertainty associated to them. Furthermore, the strongly layered nature of unconventional reservoirs demands a high-resolution representation of these properties to properly represent their behavior in simulations.

The highly layered nature and high clay content common to unconventional reservoirs produces strong anisotropy in elastic properties from layering (Backus 1962), and from the alignment of intrinsically anisotropic clay minerals (Lonardelli et al. 2007). Recently, this has been a focus for understanding the effects in hydraulic fracturing (Jiang et al. 2020; Padin et al. 2019) and several methods have illustrated the impact layered material has on energy requirements (Dontsov 2017, 2019). This strong anisotropy significantly impacts estimates of in situ stress and the design of hydraulic fracturing stimulations (Higgins et al. 2008). Also, fine layering on the scale of cm's, or less, significantly toughens rock materials to hydraulic fracture propagation by providing a means of energy dissipation at interface layer locations (Dontsov et al. 2019). Identifying, characterizing, and modeling these layers and intrinsic anisotropy is thus a fundamental component to fully and properly characterizing the rock.

As an example of these features, Fig. 1 shows the difference between a log-resolution elemental characterization of a well compared to a high-resolution elemental log from X-ray fluorescence (XRF). Although the log-resolution captures the overall character of the rock, it also misses a significant number of features clearly present at high resolution. These include interfaces between different rock facies and thin beds. The accumulation of these features influences hydraulic fracture propagation leading to decisions in the field that can be detrimental to well performance.

Typical field sonic logs can provide continuous profiles of isotropic elastic properties; however, these logs have measurement support scales on the order of 25 cm and lack sufficient independent elastic measurements to characterize anisotropic media by themselves. While triaxial measurements on core typically have support scales on the order of 2–5 cm, these measurements require intact core, and are costly and time consuming to acquire, making continuous profiling prohibitive in most cases.

This paper is a more detailed investigation of the novel methodologies introduced in Abell and Sassen (2020) for producing continuous and high-resolution (cm scale) profiles of transversely isotropic (TI) elastic properties. In that paper the authors introduced three important contributions: (1) a new experimental technique capable of providing thousands of high resolution anisotropic measurements on core in an economically feasible manner, (2) a methodology to streamline the processing of these thousands of measurements to mitigate noise and ensure physically defensible results with minimal manual intervention, and (3) a reconstruction technique that allows the extension of high resolution elastic properties to cases where only standard resolution sonic logs and a bore
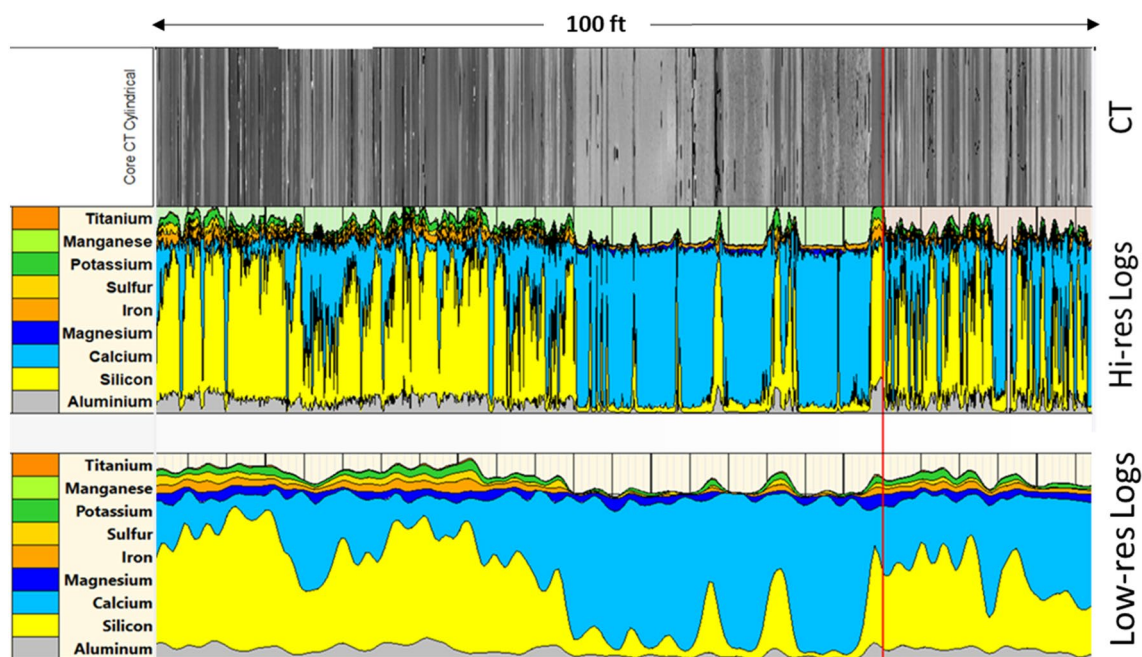

Fig. 1 Example elemental log comparing features at multiple resolutions on an unconventional core. Open-hole resolution logs (bottom) miss many of the relevant rock features that are easily captured using high-resolution logs (center). These are usually visually evident in the CT images (top)

image log are available. In this paper, we expand the discussion, applications, and verifications of those methodologies to further highlight their impact and application.

The experimental method, which utilizes piezoelectric transducers to provide high-resolution logging of core using a 6-component ultrasonic measurement (P and S at 0°, 45°, and 90° with respect to bedding) with cm support scale. These results analyze direct wave arrivals at the exposed surface of the core that allows for rapid logging with enough resolution to capture fine scale layering, and sufficient information to characterize full TI anisotropy. Here the description is expanded to illustrate the capabilities of measuring multiple orientations and how to alleviate the influence of micro-cracks typically present on vintage or desiccated core.

The methods to process the high volumes measurements using a reduced rank 3-term model of TI anisotropy based on the work of Saint Venant (1863) and later (Pouya 2007, 2011) into continuous profiles are reviewed. The utility of lower dimensional representations includes the ability to accurately describe elastic properties with limited measurements (i.e., three or four independent measurements), and the ability to de-noise full measurements (i.e., five or more independent measurements with errors). Here we provide additional insight into the statistical methodology and discussion of when a 3-term vs a more complex 4-term model is appropriate.

We also expand on the algorithmic details of how to reconstruct high-resolution TI elastic properties with the use of common field logs, and a borehole image profile to act as a structural guide. Additionally, concrete examples of the structural guide and support function are provided to compliment the field validation. This reconstruction technique greatly expands the potential for high-resolution analysis both because of the increased number of locations these logs are available verses core, and because of relatively low cost of these logs verses core.

To validate this model, we demonstrate the ability of the model to accurately fit over 12,000 ultrasonic measurement sets from various unconventional reservoirs to within noise estimates. The model is then applied to a field study where core measurements were taken and logs were available. Then, with continuous high-resolution core logging data, we compare this reduced symmetry model against a traditional regression (i.e., standard model) used to predict full five independent components of the transversely isotropic (TI) stiffness tensor. Finally, the 3-term model is used to predict full TI properties at high resolution from dipole sonic data and borehole image logs alone to illustrate a method for extending TI property estimates where core measurements are not available.

1.1 Theoretical Background

For most unconventional rock facies, the rock can be modeled as a finely bedded layered media, typically transversely isotropic (TI) media. Rocks following TI symmetry are characterized using the well-known stiffness or compliance tensor, which is expressed in Voigt notation as

$$C = \begin{vmatrix} C_{11} & C_{11} - 2C_{66} & C_{13} & & & \\ C_{11} - 2C_{66} & C_{11} & C_{13} & & 0 & \\ C_{13} & C_{13} & C_{33} & & & \\ & & & C_{44} & & \\ & 0 & & & C_{44} & \\ & & & & & C_{66} \end{vmatrix}. \tag{1}$$

For the stiffness tensor, C, and

$$C^{-1} = S = \begin{vmatrix} \frac{1}{E_1} & \frac{-\nu_{12}}{E_1} & \frac{-\nu_{31}}{E_3} & & & \\ \frac{-\nu_{12}}{E_1} & \frac{1}{E_1} & \frac{-\nu_{31}}{E_3} & & 0 & \\ \frac{-\nu_{31}}{E_3} & \frac{-\nu_{31}}{E_3} & \frac{1}{E_3} & & & \\ & & & \frac{1}{G_{31}} & & \\ & 0 & & & \frac{1}{G_{31}} & \\ & & & & & \frac{2(1+\nu_{12})}{E_1} \end{vmatrix}, \tag{2}$$

for the compliance tensor (e.g., Mavko et al. 2009). Here, E is the Young's modulus, ν is Poisson's ratio, G is the shear modulus, and the subscripts represent the Cartesian coordinates where 3 is the symmetry axis (i.e., through bedding planes). Note that the use of two subscripts represents the contraction and extension direction, respectively.

These tensors are useful in characterizing the material properties, and are most relevant in characterizing the stress, which is a leading order parameter on hydraulic fracture modeling. The effective horizontal stress, σ_1, is related to the vertical effective stress, σ_3 as

$$\sigma_1 = K_0 \sigma_3, \tag{3}$$

where

$$K_0 = \frac{\sigma_1}{\sigma_3} = \frac{E_1}{E_3} \left(\frac{\nu_{31}}{1 - \nu_{12}} \right) = \frac{C_{13}}{C_{33}}, \tag{4}$$

(Higgin et al. 2008). Thus, the motivation for understanding and characterizing the rock is especially relevant for C_{13}, which typically has the highest uncertainty of the stiffness components, and is least likely to be measured directly in laboratory testing.

Measuring these components is readily possible using ultrasonic measurements where the dynamic stiffness tensor, C_{ij}, is related to the velocities as (Pyrak-Nolte et al. 2017):

$$C_{11} = \rho V_{\text{PH}}^2, \tag{5}$$

$$C_{33} = \rho V_{PV}^2, \tag{6}$$

$$C_{44} = \rho V_{SV}^2, \tag{7}$$

$$C_{66} = \rho V_{SH}^2, \tag{8}$$

$$C_{12} = C_{11} - 2C_{66}, \tag{9}$$

$$C_{13} = \left[\frac{\left(4\rho V_{P45}^2 - C_{11} - C_{33} - 2C_{44}\right)^2 - (C_{11} - C_{33})^2}{4} \right]^{1/2} - C_{44}, \tag{10}$$

$$C_{13} = \left[\frac{-\left(4\rho V_{s45}^2 - C_{11} - C_{33} - 2C_{44}\right)^2 - (C_{11} - C_{33})^2}{4} \right]^{1/2} - C_{44}, \tag{11}$$

$$C_{13} = \left[\frac{4\rho^2\left(V_{P45}^2 - V_{s45}^2\right)^2 - (C_{11} - C_{33})^2}{4} \right]^{1/2} - C_{44}, \tag{12}$$

where ρ is the density, V_{PV}, V_{PH}, V_{P45}, V_{SV}, V_{SH}, and V_{S45} are the vertical, horizontal, and 45° P- and S-wave velocities, respectively. Equations 10–12 show different realizations of C_{13} based on whatever measurement is available (i.e., V_{p45} or V_{S45}). The C_{13} component has higher uncertainty because the 45º components used in the calculations (Eqs. 10–12) are sensitive to misalignments to bedding and is raised to 4th power greatly amplifying errors. Note that field sonic logs are typically reported in terms of slowness (i.e., DT = 1/V).

Observations have shown that many geologic materials have strong degrees of correlation between elastic properties. For example, a strong correlation between the variation of G and E in rocks. This suggests that elastic properties of these materials exist in a domain of the 5-dimensional space that defines a TI medium around a lower dimensional manifold. Therefore, there may exist lower dimension representations that will adequately describe many, but not all, TI rock materials. This use of compressing data from a large number to a smaller number of coefficients, to de-noise data, is routinely used in other disciplines such as image de-noising, signal processing, and communication (e.g., Mallat 2009; Daubechies and Heil 1992). This concept will be applied using a reduced rank model (five components reduced to three or four components) discussed below.

1.2 Measurement Methodology

This section discusses the experimental methodology for measuring the ultrasonic velocity under various polarizations along a core. It is still not the industry standard to obtain core, however, one advantage to the model methodology in this paper is the ability to measure the core in one region and propagate the results, albeit with lower certainty, to nearby well locations when high-resolution down-hole logs are available. Further discussion of this is presented in a later section.

As discussed previously (Abell and Sassen 2020), the use of a conical piezoelectric transducer (Glaser et al. 1998) is implemented to acquire anisotropic velocity measurements, while requiring a very small footprint between the source and receiver transducers (i.e., ~ 1.8 cm). Because of the small propagation distance, it is possible to acquire multiple orientations at the same location, even along a small core. As an example, measurements were made on a standard 4 in diameter core, tested on a 1/3 slabbed face, every 15°. Figure 2 highlights these results for an anisotropic section and a nearly pure carbonate section that was more isotropic.

Although the configuration, and transducer choice allows for measurements of any desired velocity orientation with respect to bedding, it is most economic to log the minimum number of measurements that still provides sufficient data for measuring TI properties. This required three orientations to bedding (i.e., horizontal, vertical, and 45°) measuring both compressional (P) and shear (S) velocities. An example of this orientation on a slabbed surface is shown in Fig. 3 along with a photograph of the experimental setup used for testing.

One of the issues with using core, is the presence of micro-cracks. This is enhanced when the core is desiccated as is the case when vintage core is being tested. One way to assist in decreasing the influence of these micro-cracks is to apply a nominal axial stress, perpendicular to the bedding, such that the micro-cracks are closed causing a significant increase in the transmitted waves. To mitigate this effect, a custom-made loading apparatus was created to apply axial load uniformly along the length of the core (Fig. 3). Figure 4 shows an example of the acquired waveforms when the source and transducer are placed on opposing sides of a visible micro-crack (i.e., vertical orientation), but within intact core, under different axial loading conditions. As the axial load is increased (i.e., different curves in Fig. 4), the waveform increases amplitude and decreases arrival time, as expected (Pyrak-Nolte et al. 1990).

For the logging performed in the laboratory, a nominal axial stress of 2000 psi is applied, unless the core condition is not sufficiently competent to withstand the load, then it is lowered to 1000 psi. Due to the change in arrival time from the loading normal to the micro-cracks, it is necessary to have some guidance on the limit of a welded micro-crack, i.e., intact rock. For this we utilized the triaxial plug (TXC) measurements, using a series of high-resolution strain gauges in a hydraulically controlled loading frame similar to Wang et al. (2020) and, when available, in situ velocity logs. The TXC measurements are typically performed on stressed
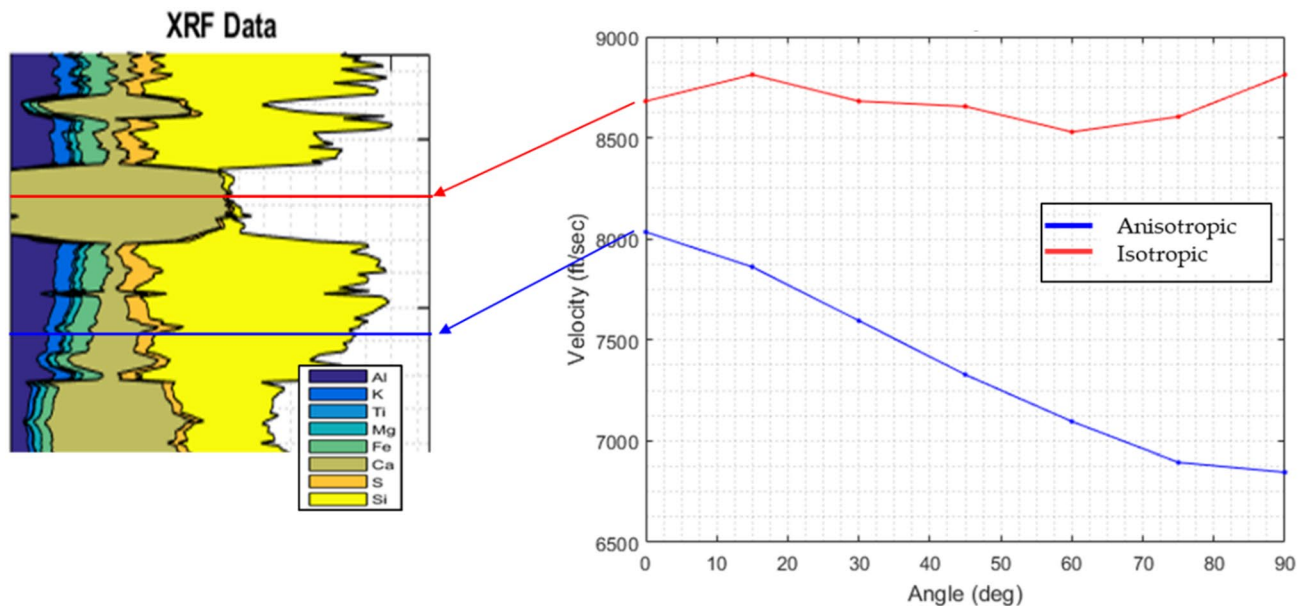
Fig. 2 Example of mineralogy data (left) from XRF scans on the core and corresponding velocity measurements in an isotropic, nearly pure carbonate section (red) and more anisotropic section (blue) demonstrating the ability to measure multiple orientations and varying degrees of anisotropy, even on a slab face
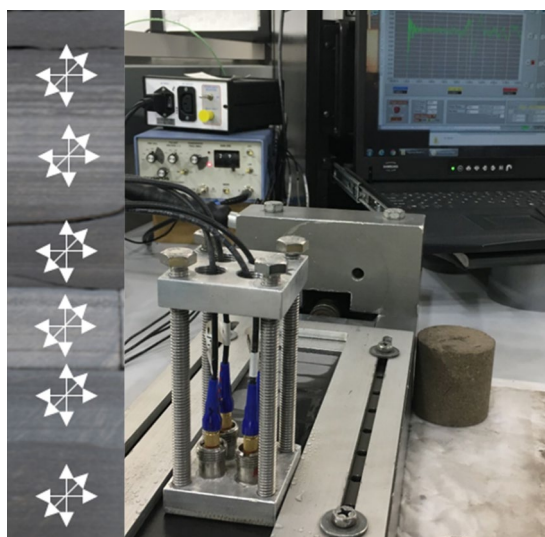

Fig. 3 Left: Examples of the fabric of the rock on the slabbed core face. The white arrows represent the measurements of ultrasonic velocities at various locations along the length of the slabbed core and at the orientations used in this study. Note that any orientation could be used based on available data and core material. Right: Experimental setup showing the transducers, electronics, and acquisition system

samples where the loading paths have been chosen to mitigate the influence from micro-cracks. Additionally, these tests are typically performed at or near the in situ stress conditions on the sample. These high-quality reference points

can be used to help train the necessary shift in velocity to in situ conditions.

As discussed previously (Abell and Sassen 2020), this methodology yields a significant number of data points along the core, typically thousands of measurement points, with reasonably low uncertainty. This is one of the main advantages of the methodology over standard logging, or even discrete point measurements (e.g., TXC velocity alone). Due to the large number of points, any erroneous measurements or non-physical values can be easily identified and statistically verified to filter out only the highest quality results.

2 Model Methodology

This section details the methods to fit core ultrasonic data to a reduced rank 3-term and 4-term model of TI anisotropy. This includes a method to construct continuous high-resolution estimates of TI elastic properties using a regression model from continuous core logging data as well as a method to predict these properties from field logs, at both standard and high-resolution. Results are contrasted against a traditional regression used to predict full five independent components of the TI stiffness tensor, and the ANNIE approximation (Schoenberg et al. 1996) when only three sonic components are available. These methods complement our core ultrasonic measurements by ensuring we have a physical and stable stiffness tensor estimate along the entire length of a core and beyond.

Fig. 4 Waveforms propagating vertically, with respect to rock bedding, along a slabbed core under various axial loads. As expected, the increased axial stress closes micro-cracks, and increases the transmitted amplitude of the propagating waves, while simultaneously decreasing the arrival time
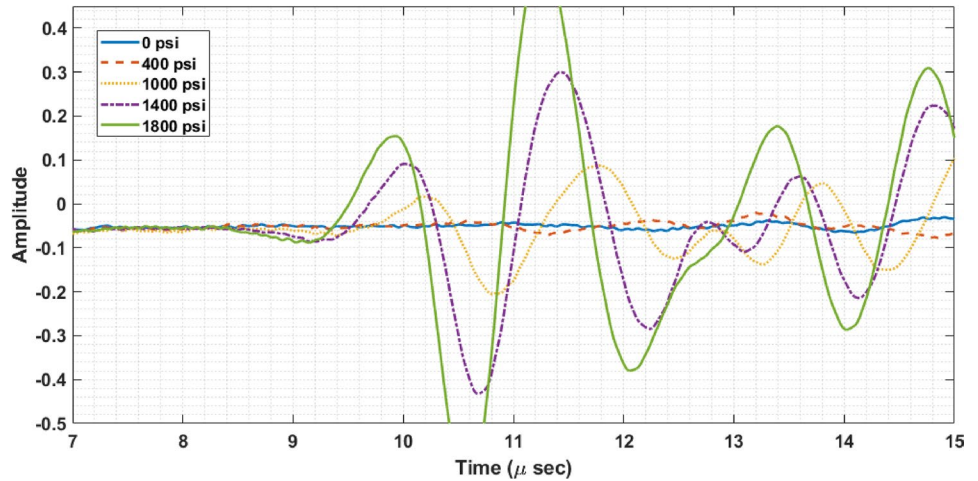
2.1 St. Venant Model

The fundamental component of the model used in this study is the ellipsoidal anisotropy introduced by St. Venant (1863), which defines symmetries not in the classic point-group anisotropies. It was later shown that these symmetries can be used to approximate layered rocks (Pouya 2007, 2011) and this model is utilized here to develop a robust method for analyzing rocks under a TI media assumption.

As introduced previously (Abell and Sassen 2020), the 3-term St. Venant model can be characterized using the compliance tensor as

$$S^{SV}\left(E_1, E_3, v\right) = \begin{vmatrix} \frac{1}{E_1} & \frac{-v}{E_1} & \frac{-v}{\sqrt{E_1 E_3}} & & & \\ \frac{-v}{E_1} & \frac{1}{E_1} & \frac{-v}{\sqrt{E_1 E_3}} & & 0 & \\ \frac{-v}{\sqrt{E_1 E_3}} & \frac{-v}{\sqrt{E_1 E_3}} & \frac{1}{E_3} & & & \\ & & & \frac{2(1+v)}{\sqrt{E_1 E_3}} & & \\ & 0 & & & \frac{2(1+v)}{\sqrt{E_1 E_3}} & \\ & & & & & \frac{2(1+v)}{E_1} \end{vmatrix}.$$

(13)

Note that the entire compliance tensor is defined by just three independent parameters: E_1, E_3, and v. These parameters are analogous to the horizontal and vertical E and isotropic v, respectively. The remainder of this paper will refer to this method as the 3-term SV model.

An extension of the 3-term model is the 4-term approximation given by

$$S^{SV}\left(E_1, E_3, v_1, v_3\right) = \begin{vmatrix} \frac{1}{E_1} & \frac{-v_1}{E_1} & \frac{-v_3}{\sqrt{E_1 E_3}} & & & \\ \frac{-v_1}{E_1} & \frac{1}{E_1} & \frac{-v_3}{\sqrt{E_1 E_3}} & & 0 & \\ \frac{-v_3}{\sqrt{E_1 E_3}} & \frac{-v_3}{\sqrt{E_1 E_3}} & \frac{1}{E_3} & & & \\ & & & \frac{2(1+v_3)}{\sqrt{E_1 E_3}} & & \\ & 0 & & & \frac{2(1+v_3)}{\sqrt{E_1 E_3}} & \\ & & & & & \frac{2(1+v_1)}{E_1} \end{vmatrix}.$$

(14)

In the 4-term SV method, both vertical and horizontal Poisson's ratio (v_3 and v_1) are used in addition to the two Young's moduli to give a total of four independent terms. This 4-term version can be utilized when four or more independent measurements of sufficient quality (discussed below) are available for more accurate approximations.

The 3-term and 4-term SV models provide a method to completely describe a TI media in cases (i) when only partial measurements of anisotropy are available (e.g., from sonic field logs), or (ii) when there are significant measurement errors on the full suite of anisotropic data (five or more components). Here, the case of finding a physically reconcilable stiffness tensors for high volume, yet higher uncertainty measurement data, from core ultrasonics, is first addressed.

The six core ultrasonic velocity components discussed above are used to calculate a TI stiffness tensor (Eq. 1) using Eqs. (5–9) and (12). If only one of the 45° components are available then Eqs. (10) or (11) are used to calculate C_{13}. Any data resulting in a stiffness tensor that does not result in a positive definite symmetric stiffness tensor is removed from the data set. The five independent parameters for the construction of the TI stiffness tensor are defined as

$$d = [C_{11}, C_{33}, C_{44}, C_{66}, C_{13}].$$

(15)

The data uncertainty is calculated using linear error propagation and from the standard deviations of the repeated ultrasonic experiments discussed in Abell and Sassen

(2020). The variance of the data uncertainties defines the diagonal of our data covariance matrix, Σ. Using a weighted least-squares cost function

$$L(x_i) = (m(x_i) - d_i)^T \Sigma^{-1} (m(x_i) - d_i), \tag{16}$$

the optimal set of model parameters, x, where $x = (E_1, E_3, \nu)$, is estimated that best fits the data, d, to within data variance using an optimizer. This measurement error-based weighting is critical because it limits the influence of unreliable measurements in the estimation process that may otherwise cause unphysical solutions. Our model output, $m(x)$, is the same five parameters of a stiffness tensor,

$$m(x) = \left[C_{11}^{SV}, C_{33}^{SV}, C_{44}^{SV}, C_{66}^{SV}, C_{13}^{SV} \right], \tag{17}$$

but calculated by the inverse St. Venant compliance tensor:

$$C^{SV} = S^{SV-1}. \tag{18}$$

The superscript SV is used to represent the 3-term or 4-term SV method. In summary we are finding the optimal reduced rank stiffness tensor that best matches our observed stiffness tensor from ultrasonic measurements.

While core ultrasonics provide us with significantly more sampling than otherwise economically achievable, the data is still insufficiently sampled to provide accurate continuous core properties due to typical core conditions. Continuous measurements would require overlapping measurements at approximately 1 cm sample spacing over intact rock. However, in many cases high-resolution continuous logging of the core (e.g., CT, XRF, DTC, spectral gamma, etc.) are also available, as is the case for the field study in this paper. These data can be used to make a predictive model of continuous elastic properties via a regression model when direct continuous sampling is not possible.

The core log data, co-located with the core ultrasonic measurements can act as the independent variable in training a regression model to predict the dependent variables of our 3-term SV model (E_1, E_3, ν) and 4-term SV model (E_1, E_3, ν_1, ν_3). The use of the St. Venant properties de-noises the data and ensures physically allowable values without individual inspection by an expert.

Approximately 12,000 collocated pairs of the dependent properties and independent properties, from unconventional core measurements, were randomly split into training (66%) and testing (33%) sets for validating the ability of the regression model to make accurate predictions on data not used in the training. After investigating several types of regression models and parameterizations, gradient boosting regression (Friedman 1999) was chosen. Following prediction of the 3-term or 4-term SV parameters, the results are used in the compliance tensor (Eq. 13) directly and can be converted to stiffness components using Eqs. (1) and (18).

To allow for three or four independent regression models, we utilize singular value decomposition (SVD) to orthogonalize the dependent parameters and minimize correlations between them as

$$\mathbf{x} = \mathbf{U}\Sigma\mathbf{V}^T. \tag{19}$$

In the SVD preprocessing the matrix x is decomposed into orthogonal left- and right-singular vectors (columns of U and V), and the singular values Σ. The singular values represent the amount of the total variation (i.e., information) described by each corresponding singular vector. The dependent variable in the regression then becomes the columns of U, and following a prediction they are transformed back to the original space using Eq. (19). We found during the model investigation phase that regression models could not predict the vector corresponding to the smallest singular value of the 4-term SV method. This indicated that the data and/or regression models are not sufficient to support the more complex 4-term model in this case. Therefore, only the 3-term SV model will be discussed from here on.

The effectiveness of 3-term SV model is analyzed by comparing it to a standard workflow. In this workflow, ultrasonic measurements are manually inspected to determine what data to remove from the training set. Then, XRF data are transformed to compositional components with the help of XRD samples. Finally, a multivariate linear regression model is trained to learn the five components of the TI stiffness tensor from co-located core logging data. The regression model order is limited to help ensure generalization out of sample. The main contrasts between these two methods are that the standard workflow uses all five terms of the stiffness tensor, and relies on manual de-noising of the data.

2.2 Estimation TI Stiffness Tensor from Down-Hole Sonic Data

Most wells do not have cored intervals, so it is important to discuss applications of this methodology to wells where only a standard suite of field down-hole measurements are available. This typically includes standard triple combo logs and ideally additional logs for high-quality anisotropic elastic property characterization from dynamic velocity measurements or nearby wells.

Using down-hole sonic data for which V_{PV}, V_{SH}, and V_{SV} data is available, there is sufficient information for fitting the 3-term SV model. The only modifications to the fitting procedures are that the data and model outputs are only looking at three terms instead of six. This modifies the input parameters from Eqs. (15) and (17) to

$$d = \left[C_{33}, C_{44}, C_{66} \right], \tag{20}$$

and

$$m(x) = \left[C_{33}^{SV}, C_{44}^{SV}, C_{66}^{SV} \right]. \tag{21}$$

Even with this simplification, the horizontal shear component is typically not available since it requires advanced multicomponent full-waveform sonic data and the extraction and processing of the Stoneley wave (White and Tongtaow 1981). When dipole shear, or any shear, is not available we can utilize empirical relationships between any available down-hole logs with sufficient resolution and information (e.g., DTC, density, gamma ray, and thermal neutron porosity) and our library of core sonic data to complete the data needed for the 3-term SV model using the above input parameters and appropriate uncertainty.

When advanced field logs are also available, including both multicomponent sonic data and image logs, it is possible to build high-resolution models on the scale of core measurements with the same relationships (Eqs. 20 and 21). However, field sonic logs have much lower spatial resolution in comparison to the core ultrasonic measurements introduced here (support of ~ 50 cm verses ~ 2 cm).

Our approach is to reconstruct high-resolution sonic profiles, z, at cm scale such that when smoothed by the measurement support of the field logs, H, they match the observations, d, to within the variance, Σ (Fig. 5). This is an ill-posed problem that requires a regularization (numerical stabilizer), and high-resolution features that are above the effective bandwidth of sonic measurements cannot be perfectly reconstructed. A typical approach of using Weiner deconvolution adds a constant to all spectral components to prevent instabilities caused by division of otherwise near-zero components during reconstruction (Gubbins 2004). This regularization approach will smooth the resulting reconstruction such that the resolution is not comparable to core data. Instead, we can build a structural constraint, ψ, from high-resolution image logs, to stabilize the reconstruction that matches observed sonic logs and honors the character of the subsurface at high resolution. The reconstruction is done by optimizing the following cost function:

$$L(z) = (H * z - d)^T \Sigma^{-1} (H * z - d) + |\psi|. \tag{22}$$

The support, H, or point spread function (psf), can either be determined from logging tool specifications on measurement support, or can be estimated from the field data by deconvolution (Andrade and Morttz-Luthi 1993). The convolution of H with the high-resolution model z produces a signal consistent with the observed low-resolution data d (see Fig. 5). The structural constraint, ψ, amounts to a guided edge preserving filter (He et al. 2013) on each sub-step of the optimization (Fig. 6). This approach allows extension of high-resolution analysis
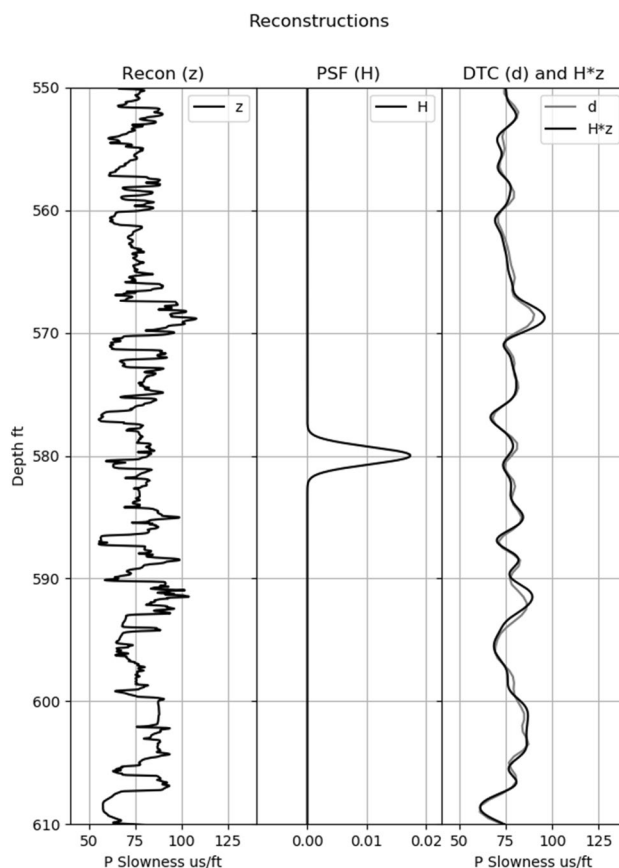
Fig. 5 Left: Example of a high resolution reconstruction. Center: The estimated psf used in the reconstruction—shifted to the center of the diagram. Right: The reconstruction smoothed by the point sread funtion (black) over the observed DTC sonic log (gray). For this case a log-scaled synthetic resistivity (SRES) derived from FMI image logs was used for the structural guide

beyond the core where these logs are available. Examples applied to the field study are discussed below.

2.3 Validation of 3-Term SV Model with Core Library

The estimation of 3-term SV properties from core ultrasonics was applied to approximately 12,000 sample locations from cores covering three unconventional basins and compared to the original data to determine the goodness of fit (Fig. 7). The goodness of fit between the observed stiffness (Eq. 15) and the estimated stiffness (Eq. 17) had an overall coefficient of determination r^2 of 0.96 (Table 1).

The coefficient of determination does not consider the uncertainty of the measurements. For that we utilized the residual Chi-squared error (χ^2), defined as the average of Eq. (16) for all sample locations, i. A value of 1 indicates a fit of the observed data to within the variance of the measurements and values less than 1 indicate that the model is
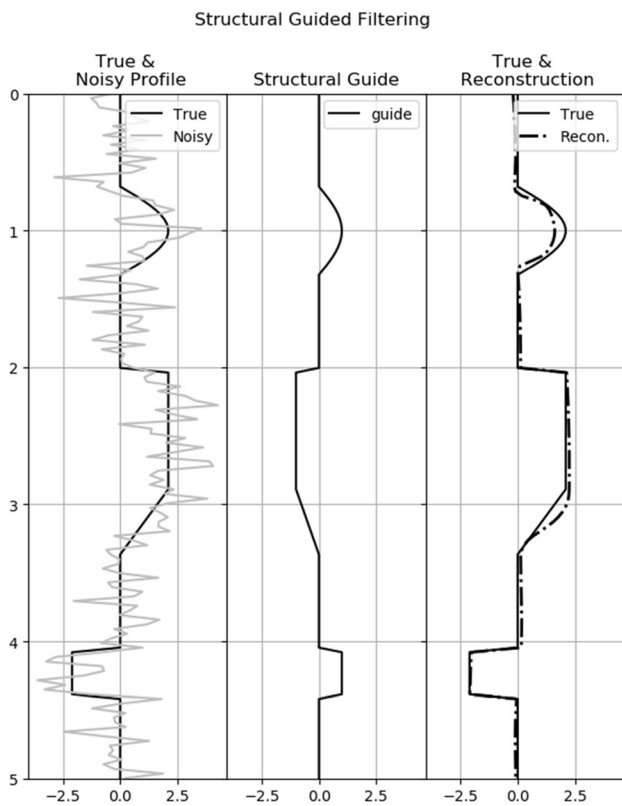
Fig. 6 Illustration of guided smoothing. During the optimization instabilities are introduced into the reconstruction from division by near-zero spectral components as illustrated by the noise in left panel. To stabilize the optimization a guided smoothing filter is used to mitigate instabilities. The resulting smoothed reconstruction follows the structure of the guide while honoring the input data. Note that the magnitude and sign of the guide are not important, but the location and character of changes are

fitting the data better than expected for the estimated variance (Taylor 1982).

One advantage to the 3-term SV model, over a standard petrophysical model, is its ability to retain physically allowable properties. Examining the distribution of Ko in Eq. (3) the raw data has many unphysical values, but following the fitting of the 3-term SV model, including the positive definite symmetric constraint, the data has effectively been de-noised and produced results that are within physical bounds and consistent with observations (Fig. 8). This is done without the need of an expert or additional processing to analyze the results.

To test the ability to reconstruct the full five terms of the stiffness tensor from only three stiffness components (C_{33}, C_{44}, and C_{66}), the same 3-term SV method was applied with Eqs. (20) and (21), and compared with the well-known ANNIE approximation (Schoenberg et al. 1996). With three observation and three unknowns, the results, shown in Table 2, nearly perfectly fit the observation (C_{33}, C_{44}, and C_{66}), but still have acceptable estimates of the critical

C_{13} component, further illustrating the usefulness of this method. Overall, the 3-term SV model fits the observation better than the ANNIE approximation with fit to C_{13} being similar in both methods.

3 Field Study

To verify the 3-term SV model, a case study on core from the Permian basin is examined. Field logs used for this analysis included: bulk density, neutron porosity, gamma ray, vertical compression slowness, vertical shear slowness, and resistivity borehole imaging. In addition to the logs acquired, the core was sampled for triaxial testing (TXC) on plugs to acquire high confidence, high-quality data at in situ stress conditions. The use of TXC results, which is standard when core analysis is performed for rock mechanics properties, were integrated with the core ultrasonic measurements, as discussed below. The anisotropic core logs, performed at lab conditions, were corrected to in situ conditions using the TXC dynamic results in addition to in situ log velocity results. This correction was previously presented and will not be further examined here (Abell and Sassen 2020).

3.1 Core Measurement Results

The experimental core ultrasonic measurements, introduced above, were acquired throughout the entire length of the cored interval for all three orientations. By examining these high-resolution results, in slowness space, the additional information gained from high resolution becomes immediately apparent. Figure 9 shows a short interval of the core where the behavior of the acoustic anisotropy has a strong agreement with the mechanical stratigraphy. The first two tracks in Fig. 9 show the CT and white light photos of the core, highlighting the presence of various facies and rock types present, common to unconventional, layered rocks. The slowness (i.e., inverse of velocity) from down-hole tools are labeled log resolution in Fig. 9 and are shown for one component of P and two components of the S. These can be directly compared to the high-resolution lab measurement tracks, where all three components are acquired.

Throughout this interval, the field logs indicate small anisotropy throughout the middle section shown as a gap between the vertical and horizontal S slowness logs in Fig. 9, and isotropic rock near the bottom of this section. Results from the lab measurements indicate that there are in fact several sections of isotropic rock (e.g., around 27 ft and 30 ft) and also several anisotropic sections (e.g., 29 ft and 31 ft). These also correlate well with the visually apparent laminations in the core images, all of which are smoothed out in the log-resolution results.

Fig. 7 Comparison of 3-term SV estimates (horizontal axis) against approximately 12,000 observed core ultrasonics samples (vertical axis) after removal of non-positive definite symmetric tensors. The diagonal line indicates the 1:1 equality line, the vertical gray lines on each sample point are the estimated standard deviation
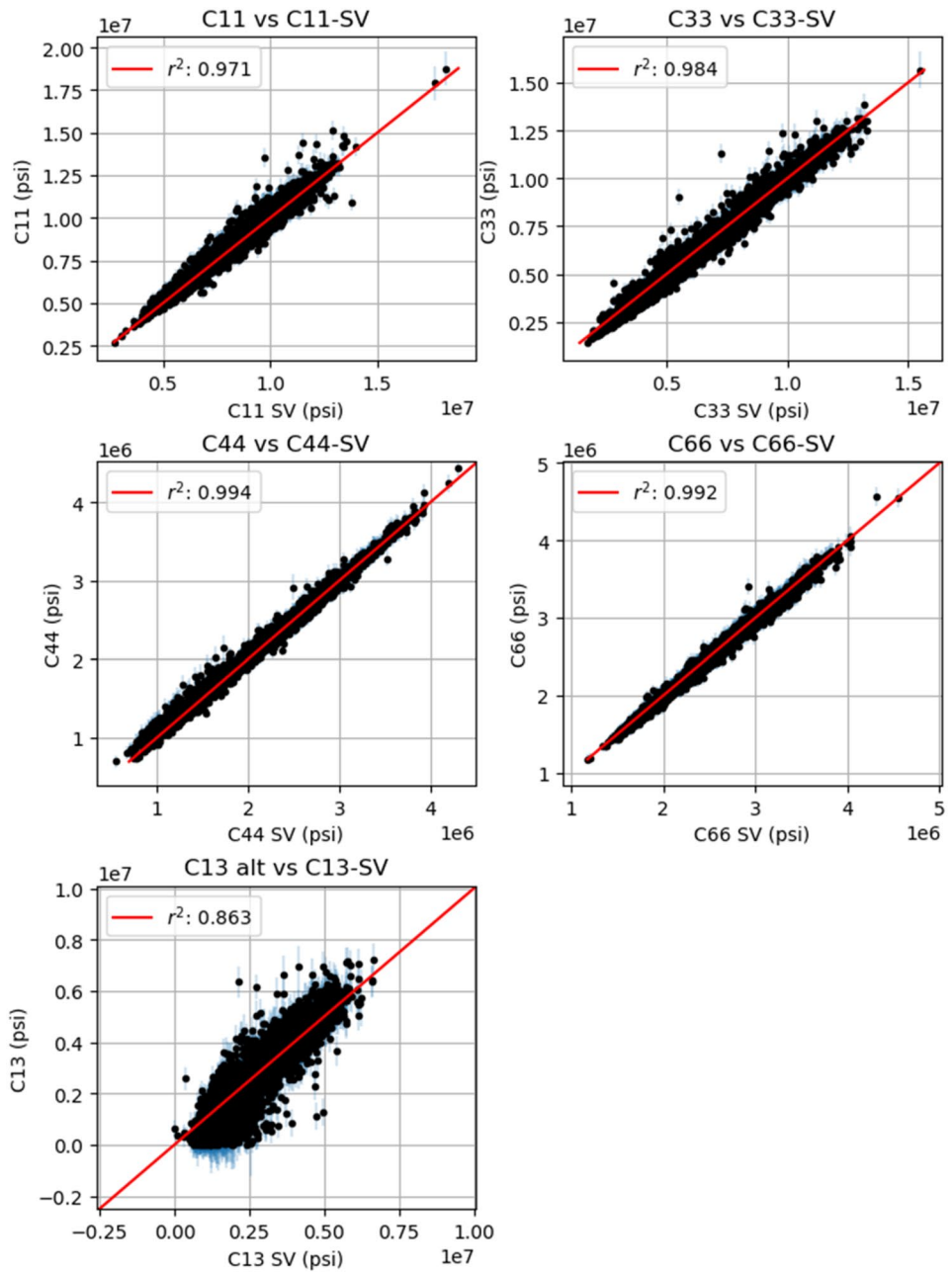

If the log resolution were to be used, the elastic properties relevant for hydraulic fracture modeling would see two blocky regions, one with high anisotropy and one with low anisotropy, instead of the numerous layers that are present even in this short section of core. These differences could have a dramatic impact on resulting hydraulic fracture modeling, which can impact field decisions. This highlights the necessity of acquiring high-resolution data to better characterize the true behavior of the rock and build a more representative model for hydraulic fracture modeling.
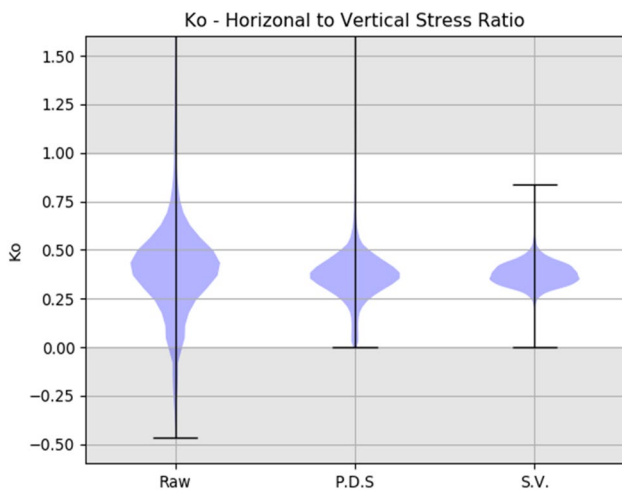
Table 1 Metrics for goodness of fit on the C_{ij} components for the 12,000 observed samples from the core ultrasonics

Component	r^2	χ^2
C_{11}	0.97	0.67
C_{33}	0.98	0.78
C_{44}	0.99	0.46
C_{66}	0.99	0.25
C_{13}	0.86	1.34
All	0.96	0.70

Fig. 8 Distribution of $K_0 = \left(C_{13}/C_{33}\right)$ for the core ultrasonic measurements (~ 12,000 samples), data filtered to only stiffness tensors that are positive definite symmetric (P.D.S.), and data filtered by the 3-term SV model (left to right). The gray regions are unphysical for geologic material and high-quality lab measurements typically range between 0.2 and 0.7

Table 2 Metrics for goodness of fit of 3-term SV when only three observations are used and the comparison to the 3-term ANNIE approximation

Stiffness Component	S.V. 3-term		ANNIE	
	r^2	χ^2	r^2	χ^2
C_{11}	0.88	2.58	0.80	8.08
C_{33}	1.00	0.17	1.00	0.00
C_{44}	1.00	0.16	1.00	0.00
C_{66}	1.00	0.07	1.00	0.00
C_{13}	0.71	1.74	0.70	2.07
All	0.92	0.94	0.90	2.03

3.2 3-Term SV Model Results

The results of the 3-term SV model, applied to the field example, was performed on the full suite of available core data as well as over sections where only log data was available, but no core was captured. This was used to illustrate the applicability of the 3-term SV method on providing a set of mechanical properties even in the absence of core.

Continuous profiles of the stiffness components from the standard model, the 3-term SV model, and the observed core ultrasonic measurements are compared in Fig. 10. Both the standard model of fitting all five independent stiffness components (dashed) and the 3-term SV model (gray) fit the observed measurements (dots) and are nearly identical in appearance and performance (Table 3). This illustrates the consistency between the two methods and further emphasizes the applicability of the 3-term SV model at capturing

the relevant elastic properties. Note that the observed data was only filtered to remove samples that failed to be positive definite symmetric tensors.

The C_{ij} results for 3-term SV model are recast in terms of dynamic E and ν using Eqs. (1) and (2). These dynamic moduli were then transformed to static moduli by a linear regression between the observed TXC measurements and the model at co-located positions. The comparison of the static moduli from the 3-term SV model and the measured TXC measurements are shown in Fig. 11. The overall results indicate a very strong data set (Table 4). The residual Chi-squared was calculated using the nominal measurement errors estimated from repeated measurements discussed above.

## 3.3 Results over Section Without Core Data

The high-resolution reconstruction method was applied to the field logs to both match the observed field logs and honor the structure of the borehole image as discussed above. These high-resolution reconstructions were then used as inputs in the 3-term SV method. To have the minimum set of three measurements, an empirical relationship using vertical compressional slowness and triple component logs was used to predict the horizontal shear component. The resulting three observations: C_{33}, C_{44}, and C_{66} were then used to estimate a full TI stiffness tensor and then converted to static moduli.

The results, shown in Fig. 12 are over an interval where the core was present to emphasize the agreement of this methodology to the actual measured results (dots in Fig. 12), although the core data was not used in this part of the analysis. This illustrates the ability to: (i) predict elastic mechanical properties where only field logs are present to within some reasonable error, (ii) append core and field results together, as is the case here, and (iii) capture fine scale variations in mechanical properties that are key to accurately estimating fracture toughness and hydraulic fracture energy balance.

4 Discussion

The core study example, discussed above, has demonstrated the applicability and resulting quality of measuring and predicting elastic mechanical properties with various levels of data inputs. The 3-term SV model has demonstrated the ability to (i) fit observed large quantities of core ultrasonics measurements, (ii) provide de-noised and physically plausible stiffness tensor, (iii) make continuous profiles of elastic properties at high resolution using core logging in conjunction with data derived from core ultrasonics and TXC measurements, and (iv) use the verified models in a predictive

Fig. 9 Highlight of a ~ 4 m section showing the difference in the log-resolution slowness measurements compared to the lab-resolution ultrasonic measurement. The small dashed line is the vertical component, the solid line is the 45° component, and the long dashed line is the horizontal component for all tracks. CT and white light photos are provided in the first two tracks for reference
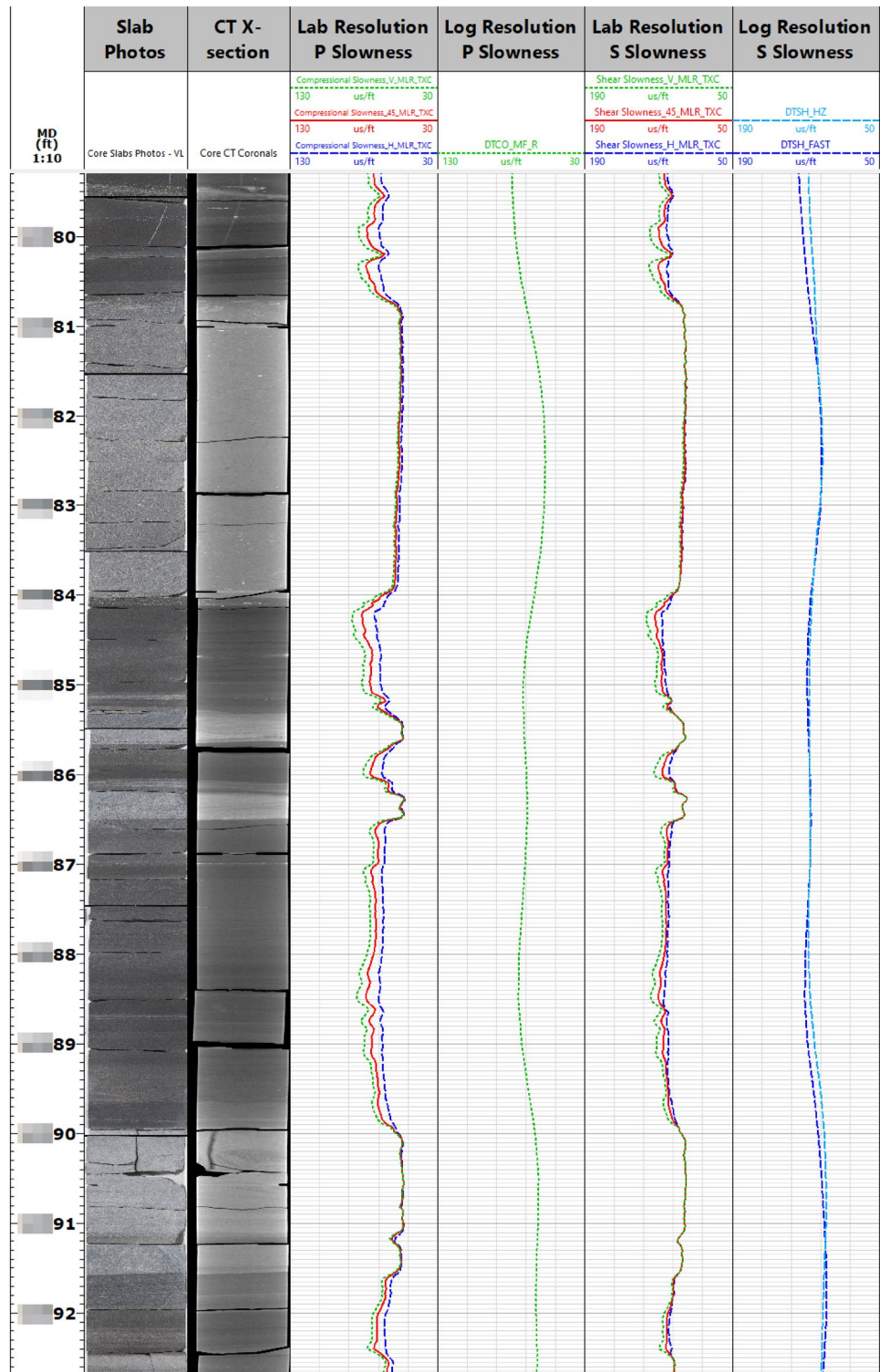
manner in wells or zones where field logging is available and core logs are not.

The estimation of reduced rank TI stiffness tensors from core ultrasonics was applied to approximately 12,000 sample locations from cores covering three unconventional basins and compared to the original data to determine the goodness of fit (Fig. 7). While we found that the data was not sufficient to support the 4-term model, for the 3-term SV model the goodness of fit between the observed stiffness (Eq. 15) and the estimated stiffness (Eq. 17) had an overall coefficient of determination r^2 of 0.96 (Table 1). The model fits these observations within the range of estimated measurement
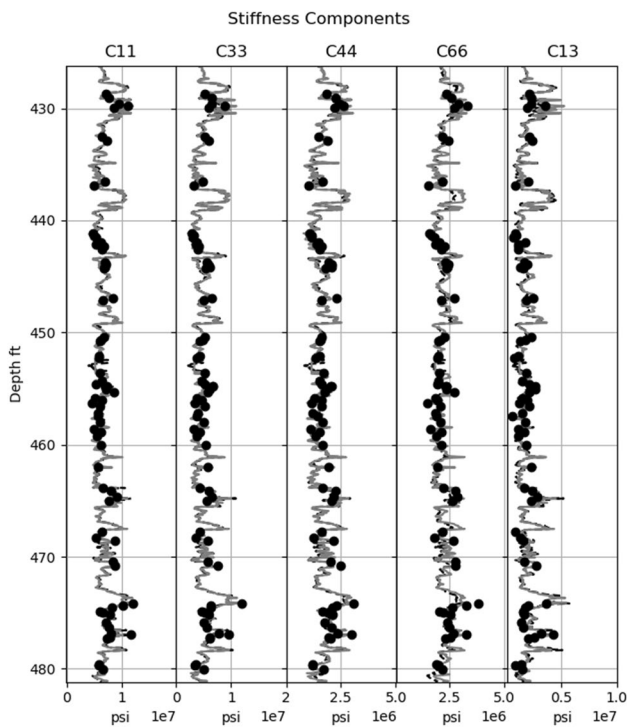
Fig. 10 Comparison between the continuous model of stiffness components from the 3-term SV regression model (solid gray) the standard regression model (black dashed line), and the observed ultrasonic measurements (black dots). Note that the 3-term SV and standard models overlap in most cases

Fig. 11 Static moduli results for both discrete TXC measurements (black dots) and 3-term SV model (gray) results over an interval showing the variation in rock types present

Table 3 Coefficient of determination (r^2) for each component of the TI stiffness tensor for both the standard and 3-term SV regression models compared with discrete anisotropic ultrasonic measurements filtered for the positive definite symmetric condition

Component	r^2 (standard)	r^2 (3-term SV)
C_{11}	0.78	0.77
C_{33}	0.78	0.77
C_{44}	0.77	0.78
C_{66}	0.74	0.80
C_{13}	0.68	0.65
All	0.75	0.75

Table 4 Metrics for goodness of fit for model to TXC measurements

Component	r^2	χ^2
E_1	0.85	1.20
E_3	0.93	0.82
v_{12}	0.76	0.80
v_{31}	0.77	1.25
All	0.83	1.05

The r^2 and χ^2 of the residual difference normalized by measurement variance

error and produces physically defensible stress estimates from the measured properties.

This indicates that the rocks in this study have a strong degree of correlation between the five independent elastic properties necessary for describing a TI media, such that a 3-dimensional representation of the properties is sufficient for describing these rocks. This is significant to the field of rock mechanics because, for these rocks, it allows reliable estimates of full TI media from measurements, even when they have significant noise or have incomplete coverage, of the five independent terms.
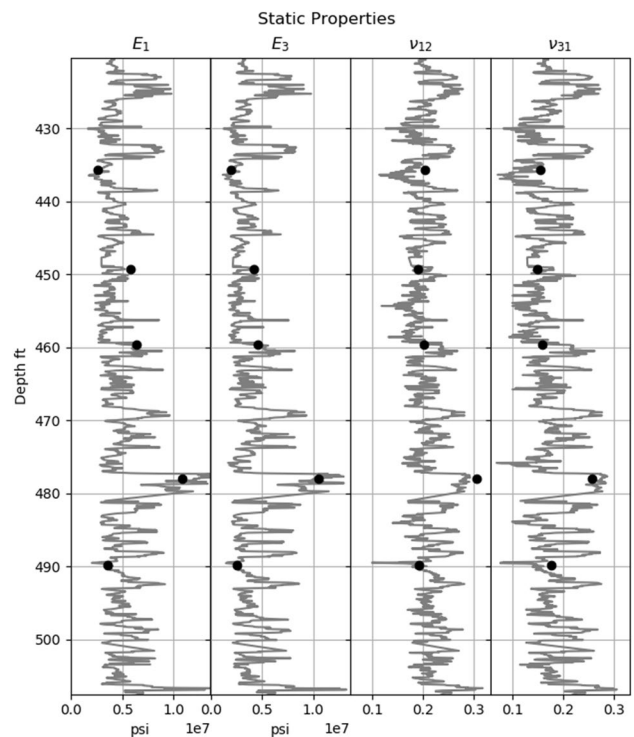
Experimentally, we demonstrated that the measurement methodology of anisotropic ultrasonic measurements, in addition to standard logging and TXC testing, provides a robust, and comprehensive high-resolution model that captures significantly more detail and features present in the rock than standard log results alone. Although these measurements, and even acquiring core, are not standard in the industry this characterization highlights the relevant features that are lost when using standard resolution field-logs alone.

The results of the standard, ANNIE, and 3-term SV models showed a highly comparable set of data with nearly identical resulting elastic properties (Tables 2, 3). This verified the applicability of the 3-term SV model in capturing the
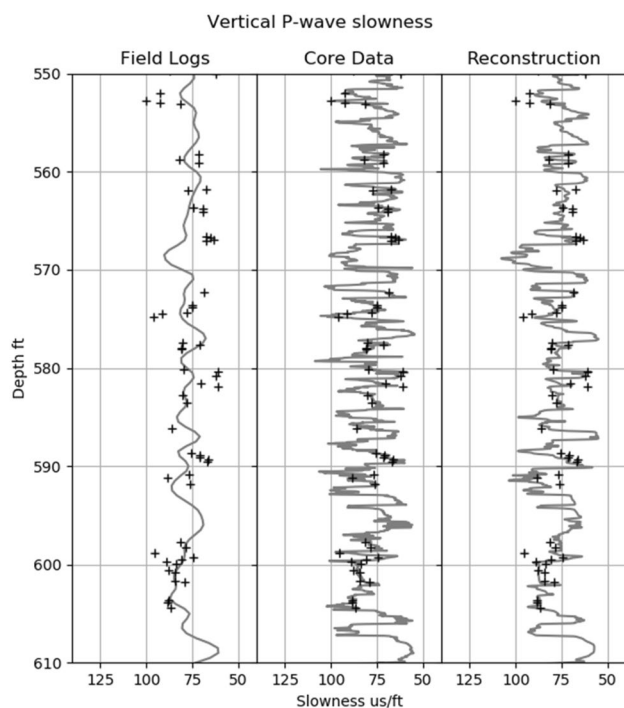
Fig. 12 Reconstruction results (right) compared with core results (center), and field logs (left) for the vertical compressional slowness. The black crosses are the discrete ultrasonic measurements

variability observed in the rock facies both where core data and field data are available.

Results using only three components from field logs were comparede to the high-resolution measurements over the cored interval (Fig. 12). Comparisons of the 3-term SV model using the high-resolution core logs versus the downhole logs and high-resolution field image logs illustrates that this methodology is robust at capturing the relevant features of the rock even with fewer inputs into the model. Because most wells have only field logs, this is the most useful application of the methodology presented here. Using the available data and this novel model, a complete prediction can be acquired and provide higher quality, more reliable elastic mechanical property inputs—at high resolution. The ability to reconstruct the fine scale contrasts in mechanical properties is critical to accurately accounting for fracture toughness and hydraulic fracture energy balance within a hydraulic fracture simulation.

5 Conclusion

Methodologies for integrating discrete data from core logs, including anisotropic core ultrasonic logging, were introduced, and applied to a core from the Permian basin to demonstrate the quality and type of results available from

these measurements. These models provided high-resolution elastic properties consistent with detailed observations on the rock and allow for a higher quality, higher resolution input data set, which better represents the rock, to hydraulic fracture modeling than is typically available.

Since it is not industry standard to acquire core, an extension of this methodology was presented that allows the use of field logs and any available nearby high-resolution data (e.g., core or image logs) to predict, at high resolution, the mechanical properties of a given well of interest in a new area. We demonstrated that this produced results consistent with core measurements. This is perhaps the most immediately relevant to the industry and illustrates the robustness of the St. Venant methodology when properly integrated with data science.

A regression model to learn three independent components of a modified 3-term SV model, was compared to the standard model, which utilizes five independent MLRs to learn the five stiffness tensor components. Both approaches gave very similar results (both with overall $r^2 = 0.75$) when compared to the observed stiffness components.

The main advantages of the 3-term SV model were the need for substantially less time to prepare the data for training, consistent output regardless of the individual analyzing the results, automatic filtering and de-noising, and highly consistent results that do not have bias from the individual components.

Currently, both whole core analysis, advanced sonic logs, and borehole image logs are not the industry standard yet the requirement for high confidence hydraulic fracture modeling is. As this paper has demonstrated, the typical low-resolution field logs miss a significant amount of variation in the rock. The absence of this high-resolution data can severely impact hydraulic (He et al. 2013) fracturing results, leading to completion designs that over or under-stimulate the reservoir of interest ultimately having an impact on production.

Declarations

References

Abell B, Sassen S (2020) Mechanical logs for hydraulic fracture modeling-honoring rock fabric with high resolution data. In: 54th US rock mechanics/geomechanics symposium, ARMA, Golden

Andrade A, Morttz-Luthi S (1993) Deconvolution of wireline logs using point-spread function. In: 3rd International Congress of the Brazilian Geophysical Society. European Association of Geoscientists & Engineers. https://doi.org/10.3997/2214-4609-pdb.324.866

Backus GE (1962) Long-wave elastic anisotropy produced by horizontal layering. J Geophys Res 67(11):4427–4440

Daubechies I, Heil C (1992) Ten lectures on wavelets ingrid. Comput Phys. https://doi.org/10.1063/1.4823127

Dontsov E (2017) A homogenization approach for modeling a propagating hydraulic fracture in a layered material. Geophysics 82(6):MR153–MR162

Dontsov E (2019) Scaling laws for hydraulic fractures driven by a power-law fluid in homogeneous anisotropic rocks. Int J Numer Anal Methods Geomech 43:519–529

Dontsov E, Bunger A, Abell B, Suarez-Rivera R (2019) Ultrafast hydraulic fracturing model for optimizing cube development. In: Unconventional resources technology conference, Denver. https://doi.org/10.15530/urtec-2019-884

Friedman J (1999) Greedy function approximation: a gradient booting machine. IMS Reitz Lecture

Glaser S, Weiss G, Johnson L (1998) Body waves recorded inside an elastic half-space by an embedded, wideband velocity sensor. J Acoust Soc Am 104(3):1404–1412

Gubbins D (2004) Time series analysis and inverse theory for geophysicists. Cambridge University Press, Cambridge. https://doi.org/10.1017/CBO9780511840302

He K, Sun J, Tang X (2013) Guided image filtering. IEEE Trans Pattern Anal Mach Intell 35(6):1397–1409. https://doi.org/10.1109/TPAMI.2012.213

Higgins S, Goodwin S, Donald A, Bratton T, Tracy G (2008) Anisotropic stress models improve completion design in the Baxter shale. In: SPE annual technical conference, Denver, pp 1–10

Jiang L, Yoon H, Bobet A, Pyrak-Nolte L (2020) Mineral fabric as a hidden variable in fracture formation in layered media. Sci Rep. https://doi.org/10.1038/s41598-020-58793-y

Lonardelli I, Wenk H, Ren Y (2007) Preferred orientation and elastic anisotropy in shales. Geophysics 72(2):D33–D40

Mallat S (2009) A wavelet tour of signal processing (third edition): chapter 11 - denoising. Academic Press, pp 535–610. https://doi.org/10.1016/B978-0-12-374370-1.00015-X (**ISBN 9780123743701**)

Mavko G, Mukerji T, Dvorkin J (2009) The rock physics handbook: tools for seismic analysis of porous media, 2nd edn. Cambridge University Press, Cambridge. https://doi.org/10.1017/CBO9780511626753

Padin A, Pijaudier-Cabot G, Lejay A, Pourpak H, Mathieu J, Onaisi A, Boitnott G, Louis L (2019) High-resolution measurements of elasticity at core scale. Improving mechanical earth model calibration at the Vaca Muerta formation. In: Unconventional resources technology conference, Denver, p 13. https://doi.org/10.15530/urtec-2019-A-121-URTeC

Pouya A (2007) Ellipsoidal anisotropies in linear elasticity extension of Saint Venant's work to phenomenological modelling of materials. Int J Damage Mech 16:95–126

Pouya A (2011) Ellipsoidal anisotropy in linear elasticity: approximation models and analytical solutions. Int J Solids Struct 48:2245–2254. https://doi.org/10.1016/j.ijsolstr.2011.03.028

Pyrak-Nolte L, Myer L, Cook N (1990) Transmission of seismic waves across single natural fractures. J Geophys Res 95(B6):8617–8638

Pyrak-Nolte L, Shao S, Abell B (2017) Elastic waves in fractured isotropic and anisotropic media. In: Feng X (ed) Rock mechanics and engineering, chap. 11, vol 1. CRC Press/Balkema, London, pp 323–361

Saint Venant B (1863) Sur la distribution des elasticites autour de chaque point d'un solide ou d'un milieu de contexture quelconque, particulierement lorsqui'il est amorphe sans etre isotrope. Journal De Math Pures Et Appliquees VIII:257–430

Schoenberg M, Muir M, Sayers C (1996) Introducing ANNIE: a simple three-parameter anisotropic velocity model for shales. J Seism Explor 5:35–49

Taylor J (1982) An introduction to error analysis: the study of uncertainties in physical measurements. University Science Books, Mill Valey

Wang Y, Li H, Mitra A, Han DH, Long T (2020) Anisotropic strength and failure behaviors of transversely isotropic shales: an experimental investigation. Interpretation 8(3):1A–Y1. https://doi.org/10.1190/INT-2019-0275.1

White JE, Tongtaow C (1981) Cylindrical waves in transversely isotropic media. J Acoust Soc Am 70:1147